Computer Modeling of Polyleucine-Based Coiled Coil Dimers in a Realistic Membrane Environment: Insight into Helix−Helix Interactions in Membrane Proteins†

Walter L. Ash, Thomas Stockner, Justin L. MacCallum, and D. Peter Tieleman*

Department of Biological Science, University of Calgary, 2500 University Drive NW, Calgary, Alberta T2N 1N4, Canada

Received March 18, 2004; Revised Manuscript Received April 30, 2004

ABSTRACT: Simulated annealing was performed to model parallel dimers of α-helical transmembrane peptides with the sequence $L_{11}XL_{12}$, predicting left-handed coiled coil geometry in all cases. Insertion of peptides containing threonine, asparagine, alanine, phenylalanine, and leucine in position 12 into realistic model membranes showed these structures were stable for 20 ns of molecular dynamics simulation time. Threonine could participate in intermolecular hydrogen bonds, but predominantly formed hydrogen bonds to the backbone of the helix it resided on. These hydrogen bonds, although infrequent, appeared to promote closer association of polyleucine helices. Asparagine participated in multiple, rapidly fluctuating intermolecular and intramolecular hydrogen bonds, and may have slightly destabilized optimum van der Waals packing in favor of optimum hydrogen bonding. Coordinated rotations of transmembrane helices about their axes were observed, indicating helices may rotate around one another during the folding of membrane proteins or other processes. These rotations were inhibited by phenylalanine, suggesting a role for bulky residues in modulating membrane protein dynamics.

Membrane proteins have numerous important physiological roles, including the transport of solutes and macromolecules, intercellular signaling, cell−cell recognition, and the compartmentalization of important cellular processes such as in respiration. Many membrane proteins are composed of α-helical membrane-spanning segments, often in bundles connected by loops or soluble domains. Examples of these include the G protein-coupled receptors (*1*), ligand and voltage-gated ion channels (*2*, *3*), and small multidrug resistance proteins such as EmrE (*4*). Bitopic membrane proteins such as glycophorin A (GpA)[1] and the receptor tyrosine kinases (e.g., ErbB2), comprising homodimers of single transmembrane segments that can associate independently of extramembranous domains, have also been characterized (*5*).

In general, membrane proteins are difficult to study using established atomic-resolution structural methods commonly applied to water-soluble proteins, particularly nuclear magnetic resonance spectroscopy and X-ray diffraction. Fortunately, the membrane environment and biomolecular insertion processes impose constraints that can be exploited to predict structural properties in the absence of other structural information (*6*−*8*). Theoretical examinations and experiments now allow determination of such factors as the number and orientations of transmembrane helices, the side-chains involved in helix−helix packing interfaces, sequence location of helix termini at the lipid−water interface, cytoplasmic or extracellular localization of N-, C-termini and loops, and spatial distances in the folded protein between specific residues (*9*−*11*).

In 1990, Popot and Engelman proposed a two-stage model for the folding of these proteins (*7*, *12*), by which α-helices are first inserted into the membrane, and then associated to form a functional bundle. The basis of this model is the assumption that individual α-helices form independently stable domains, a suggestion that is well supported by theory and experiment (*5*, *13*). This observation is rationalized by considering the increased strength of backbone hydrogen bonds, and hydrophobic matching of nonpolar side-chains with lipid acyl chains in the membrane interior, and the model of progressive insertion of helices into the lipid bilayer during translocation (*7*, *13*).

This model is admittedly incomplete, as it does not account for the binding of cofactors or other protein loops and domains (*7*, *13*), kinks, or hinges induced by proline (*14*) or other distortions from α-helicity, and specific binding of lipids (*15*). Furthermore, it is only an approximation of the more complex equilibrium dynamics involved in folding (*16*). Nevertheless, the simplicity and general applicability of this model suggest that the current major challenge for membrane protein structure prediction and design is to understand the forces driving and specifying helix−helix interactions in membranes.

† D.P.T. is an Alberta Heritage Foundation for Medical Research (AHFMR) Scholar. W.L.A. is supported by an AHFMR studentship. J.L.M. is supported by studentships from the Natural Sciences and Engineering Research Council and Alberta Ingenuity. Work in our laboratory is conducted in part with resources of the Western Canada Research Grid (WESTGRID).

* Corresponding author. E-mail: tieleman@ucalgary.ca; fax: (403) 289-9311; phone: (403) 220-2966.

[1] Abbreviations: DOPC, 1,2-dioleoyl-*sn*-glycero-3-phosphocholine; GpA, glycophorin A; MD, molecular dynamics; ns, nanosecond(s); OPLS, optimized parameters for liquid simulations; PME, particle mesh Ewald; RMSD, root-mean-squared deviation; SAMD, simulated annealing and restrained molecular dynamics; SPC, simple point charge.

10.1021/bi0494572 CCC: $27.50
Published on Web 06/22/2004

Several helix−helix interaction motifs have been recognized (*17*, *18*), although the bases by which they promote specific association are not completely understood. Some general force driving helix association may favor aggregation of helices (*19*−*21*), with the specificity and stability of these aggregates dictated by detailed fit between complementary surfaces (*7*) and electrostatic interactions (*18*) between backbones or side-chains. The latter are shown to strongly promote aggregation, possibly at the expense of specificity (*22*, *23*). Point mutations to hydrophilic amino acids have been implicated in diseases, for example, the mutation valine-664 to glutamine (V664E) which activates the oncogene neu/erbB2 (*24*, *25*), and the harmful V232D mutation in TM4 of the cystic fibrosis transmembrane conductance regulator (*26*).

Various methods for predicting the association of transmembrane helices have been developed. Some modelers have elected to use detailed atomic interaction functions with global searching methods to predict the proper association of α-helices (*27*, *28*), sometimes in conjunction with experimental, evolutionary, and/or mutagenesis data (*5*). These predictions have often been done in vacuo as an electrostatic approximation of the low dielectric environment in the bilayer interior (*29*). Other studies have used molecular dynamics simulations in fully represented lipid bilayers to develop models of membrane protein structure or function (*30*−*32*), for example, the pore forming antimicrobial peptide alamethicin (*33*). Two recent studies have employed an empirical helix−helix interaction function based on an estimate of the interface burial propensity of various amino acids. These studies successfully predicted the conformation of the glycophorin A dimer (*34*), for which NMR structures exist, and suggested a mechanism for activation of the ErbB2 epidermal growth factor receptor dimer (*35*) consistent with available experimental data. The use of numerous approaches with the selection of consensus models is also a powerful technique (*36*). Despite these limited successes, there is no method that consistently and accurately predicts the tertiary structure of membrane proteins from sequence, or conversely can design a membrane protein sequence around a desired tertiary structure. Many experiments on model peptide systems have been undertaken in an effort to better understand the behavior of transmembrane proteins.

Model Transmembrane Helices and Coiled Coils. In accordance with the two-stage model, the folding of polytopic membrane proteins appears to occur in a manner analogous to the association of single membrane spanning α-helices (*37*). Taking advantage of this analogy, simpler model transmembrane helices have been studied in an effort to elucidate the factors determining specificity of helix−helix interactions in membrane proteins. These include the designed peptide MS1 (*38*), serine and threonine containing transmembrane helices (*39*), the WALP and KALP series of leucine-alanine repeat peptides (*40*), and polyleucine-based peptides (*41*−*43*).

MS1 is based on a segment of the bZIP transcription factor GCN4 (*38*) from *Saccharomyces cerevisiae*. The crystal structure of GCN4 (*44*) shows two helices wrapped around one another in a left-handed coiled coil (*45*), and the sequence of this region exhibits a characteristic seven-residue "heptad repeat" of leucines (Figure 1). This leucine zipper motif is characteristic of other members of the bZIP class of transcription factors (*46*).

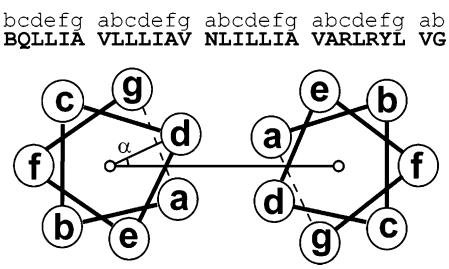

FIGURE 1: A coiled coil is shown in a helical wheel representation, in the rotating frame of the supercoil. The positions in the packing interface are defined by the labels "a" through "g" and are characterized by the "crick angle" α. The sequence of the designed transmembrane helix MS1 is shown, with amino acid packing positions labeled according to the structure of the GCN4 leucine zipper on which MS1's sequence is based. A heptad repeat of leucines in position "d" and valines in position "a" is apparent.

SDS−PAGE, fluorescence resonance energy transfer, and analytical ultracentrifugation experiments demonstrate that MS1 transmembrane helices associate when they contain polar, hydrogen-bonding substitutions, in particular, those containing the carboxyl and amide functions: asparagine, aspartate, glutamine, and glutamate (*22*). This driving force appears to be strongest when asparagine is placed in the sequence such that it lies in the center of the bilayer rather than near the headgroup regions, an observation that is reflected in the bilayer-centered location of asparagines in solved membrane protein structures (*47*). Polyleucine transmembrane helices have also been shown to associate in SDS when they contain the same polar hydrogen-bonding residues (*23*), although there is evidence that purely hydrophobic polyleucine-based sequences can also associate to a lesser degree (*48*). Polyleucine peptides fused to staphylococcal nuclease exist as monomers and homodimers in SDS−PAGE experiments.

Analyses of membrane protein structures in the Protein Data Bank have shown that pairs of α-helices in transmembrane proteins can also participate in coiled coil packing (*49*, *50*), and numerous transmembrane segments containing a heptad repeat of hydrophobic amino acids have been identified and shown to associate in vivo (*42*). Because MS1 is based on GCN4, it is plausible that MS1 may exhibit coiled coil packing in the membrane. By extension, the polyleucine peptides may also form coiled coils.

Goals and Approach. The goals of this study are to determine whether the canonical coiled coil packing of leucine interfaces in soluble proteins is a reasonable structure for the polyleucine dimer in a membrane, and to investigate the effects of specific amino acid substitutions on the structure and dynamics of this dimer. This could be expected to give insight into the effects of these amino acids on the packing of real membrane proteins.

An in vacuo simulated annealing and molecular dynamics (SAMD) protocol (*51*) was employed to generate 450 dimers of each of Ace-L_{11}-X-L_{12}-NH_2 with the following amino acid substitutions: alanine (*ala*), leucine (*leu*), phenylalanine (*phe*), asparagine (*asn*), and threonine (*thr*). These were ranked by symmetry, potential energy, and a clustering analysis. Because the lipid environment can have a very

strong effect on the structure and behavior of many membrane proteins (*52*), fully detailed simulations were desirable to provide better evidence for the structural insight gained from SAMD. Furthermore, the dynamic behavior of these peptides could be investigated in a detailed molecular dynamics simulation, which is not possible with SAMD. The highest ranked structures were independently inserted into a model 1,2-dioleoyl-*sn*-glycero-3-phosphatidylcholine (DOPC) membrane and simulated for 20 ns—one each of *ala*, *leu*, *phe*, and *asn*, and two *thr* simulations. The two *thr* simulations were performed to assess the differences between threonine in a peptide dimer interface (*thr1*) and threonine exposed to lipid (*thr2*). Thus, the effects of small, aromatic, amide containing, and hydroxyl containing amino acids on the structure and dynamics of polyleucine were investigated.

Threonine is interesting because it is known to form intramolecular hydrogen bonds to the helical backbone in many transmembrane helices (*50*), it is important in stabilizing the GpA dimer (*53*), and it has only a slight effect on the dimerization behavior of polyleucine (*23*) unless introduced in multiple positions (*39*). Analysis of the differences in inter- and intramolecular hydrogen bonding between threonine side-chains exposed to lipid and those positioned in a protein dimerization interface might lend insight into whether a hydrogen-bonding interaction affects this association-promoting behavior. Unlike threonine, a single asparagine mutation is known to stabilize polyleucine and MS1 dimers and higher-order aggregates. Smaller amino acids are more common in helix−helix interfaces, but the introduction of alanine destabilizes polyleucine interactions (*48*). Phenylalanine was included to assess whether this bulky amino acid induces structural rearrangement, since it was frequently identified in self-associating synthetic hydrophobic transmembrane helices (*42*).

For simplicity, only dimers with the same N- to C-terminal directionality (parallel dimers) were analyzed in this study. We make the assumption that the results from the parallel case can be generalized to the antiparallel case, once intrinsic differences between parallel and antiparallel packing are understood. Both parallel and antiparallel coiled coils exhibit similar steric packing interactions (*49*), although the latter arrangement might be favored by smaller residues (*54*, *55*). We also make the simplifying assumption of symmetry during the initial stages of dimer generation, which seems reasonable in light of the symmetry of other known transmembrane helix dimers and soluble coiled coils (*5*, *56*).

METHODS

SAMD. The sequences analyzed were (Ace-$L_{11}XL_{12}$-NH_2), with X = alanine (*ala*), leucine (*leu*), phenylalanine (*phe*), threonine (*thr*), and asparagine (*asp*). Simulated annealing was performed using the Crystallography and NMR System (*57*) using the OPLS force field (*58*) and techniques similar to those described by other researchers (*36*, *51*, *59*). For each sequence, 25 structures were generated from each of 18 perfectly parallel and symmetric starting configurations for a total of 450 structures. Starting configurations were generated with the α-carbon of the mutated residue (position 12) covering an evenly distributed range of orientations with a maximum crick angle (see Figure 1) of ± 72 degrees.

Table 1: Average Helix−Helix Crossing Angles and Coiled Coil Radii from Simulations of Dimers in DOPC; Heptad Assignments of the Variable Residue at Sequence Position 12

	crossing angle (°)		radius (nm)		
simulation	average	std dev	average	std dev	heptad[a]
ala	23.01	3.36	0.492	0.13	d/d
asn	20.88	2.66	0.504	0.11	d/d
leu	18.01	2.72	0.523	0.15	d/d
phe	20.07	3.50	0.513	0.13	d/d
thr	24.75	3.04	0.471	0.15	a/a
thr2	19.93	3.71	0.512	0.15	e/e

[a] Heptad positions were assigned using the TWISTER algorithm (*61*) and are based on the position of the side-chain defined by the crick angle (α, Figure 1).

Harmonic restraints were used to enforce α-helical hydrogen bonding patterns by applying a penalty if backbone hydrogen bond (O−H) lengths exceeded 0.32 nm, a value much larger than observed in the final structures. A single restraint was applied between the centers of mass of the two helices, applying a weak penalty on distances exceeding 1.14 nm.

Ranking structures was a three-step process. First, all structures were clustered based on backbone atom coordinates using NMRCLUST (*60*) with an RMSD cutoff of 0.1 nm. Second, a modified version of TWISTER (*61*) was used to assess symmetry. The symmetry score was calculated by rotating the entire structure 180 degrees around the average vector defined by the coiled coil axis, then calculating the C_α coordinate root-mean-squared deviation (RMSD) between rotated and initial structures. The clustering results were filtered by removing those 50% of structures that had the lowest symmetry scores. Finally, the best models from each of the 10 largest remaining clusters were picked based on their potential energy scores.

Simulations in a Bilayer. Only one configuration of each sequence was simulated, except for two threonine simulations: *thr* with threonine occupying an "a" position in the interface (Figure 1), and *thr2* with threonine outside of the dimer interface in the "e" position. These were done to assess the differences in hydrogen bonding behavior between interfacial and lipid exposed threonine residues. Simulations were performed with GROMACS 3.1.4 (*62*) and the OPLS all atom protein force field (*58*) with the lipid parameters of Berger et al. (*63*) and GROMACS parameters for the oleate unsaturated bond (*64*). All simulations used periodic boundary conditions, Lennard-Jones and short-range electrostatics cutoffs of 1.0 nm, particle mesh Ewald (PME) summation (*65*) with order 4 spline interpolation and a 0.12-nm grid, and a neighborlist update every 10 steps. Temperature was set to 300 K using a Berendsen thermostat (*66*) ($\tau = 0.1$ ps) coupling separately to protein, water, and lipid. After equilibration, Berendsen semiisotropic pressure coupling was used with a compressibility of 4.5×10^{-5} (bar^{-1}) in both the membrane plane and perpendicular to the bilayer with a reference pressure of 1 bar. The highest ranking peptides from SAMD that contained the mutant residue in either an "a" or "d" position (Table 2) were inserted with a molecular dynamics hole-generating protocol (*67*), described below, into an equilibrated bilayer in a box containing 58 DOPC molecules and 2807 SPC water molecules (Figure 3).

Initially, five lipids with phosphorus atoms within 0.7 nm of the center of the bilayer plane and one additional lipid

Table 2: Hydrogen Bond Types and Prevalence Observed in the Threonine and Asparagine Containing Dimers Simulated in DOPC

hydrogen bond type[a]	*asn* (%)	*thr* (%)	*thr2*[b] (%)
SC1-BB2	22.6	0	0
SC1-BB1	55.4	91.9	99.5
SC1-SC2	44.5	23.3	0
SC2-BB1	30.2	0	0
SC2-BB2	45.5	86.3	99.3
inter >= 1	99.0	23.3	0
intra >= 1	64.5	99.9	99.9

[a] Hydrogen bond types are labeled as follows. SC: side-chain, BB: backbone of chain; numbers specify monomer 1 or 2. Inter/intra >= 1: at least 1 inter/intramolecular hydrogen bond is present. [b] The threonine side-chains in this dimer were positioned outside of the helix−helix interface, precluding the formation of any intermolecular hydrogen bonds.

(to create a symmetric bilayer) were removed from a 64 DOPC bilayer, resulting in a membrane with a small cavity of insufficient size to incorporate a polyleucine dimer. Solvent-accessible surfaces of the peptide dimers were generated with MSMS (*68*) using a probe radius of 1.4 Å and a surface density of 0.34 vertices/Å^2. These were translated to the center of the bilayer and used as input for a modified version of GROMACS 3.1.4 that applied a force to lipid atoms perpendicular to the molecular surface (*67*) with a force constant of 25 kJ mol^{-1} nm^{-1}. The forces on peptide-surface penetrating atoms were averaged over all atoms in a molecule to avoid lipids straddling the protein inclusion. Lipid phosphorus atoms were restrained normal to the bilayer plane with a force constant of 1000 kJ mol^{-1} nm^{-1} and water molecules were excluded from a slab 2.1 nm thick centered in the bilayer with a force constant of 7.5 kJ mol^{-1} nm^{-1}. The total simulation time during this stage was 20 ps, in 1×10^4 MD steps, which was sufficient to generate a hole that conformed reasonably well to the shape of the protein inclusion. It was found that in some cases several atoms in a lipid acyl chain had to be moved manually after hole generation (~0.1 nm total distance) in cases of overlap with a peptide side-chain in a manner that could not be resolved with energy minimization, for example, by being stuck in a cleft formed by protein side-chain atoms. These overlaps were not very deep (~0.1 nm) and involved ca. 3−6 methylene groups. Subsequent energy minimization and 1-ns simulations with harmonic restraints on all protein atoms were used to produce starting structures for the 20-ns simulations. These simulations took approximately 45 days, with each simulation running on an Intel Pentium III 1-GHz processor.

Analysis. All coiled coil radii, crossing angles, and helix rotations (crick angles) were calculated with the TWISTER algorithm (*61*), averaging over eight core residues to remove possible noise due to helix termini fluctuations. The average crick angle (Figure 9) was calculated over residues 9−15 of each monomer, for a total of seven residues surrounding and including the variable amino acid. Secondary structure was calculated using DSSP (*69*), and hydrogen bonding analysis employed the geometric criteria defined by DSSP (donor−hydrogen−acceptor angle cutoff: 60°, hydrogen−acceptor distance cutoff: 0.25 nm). Snapshots were rendered using VMD (*70*). Variational cross correlation was calculated

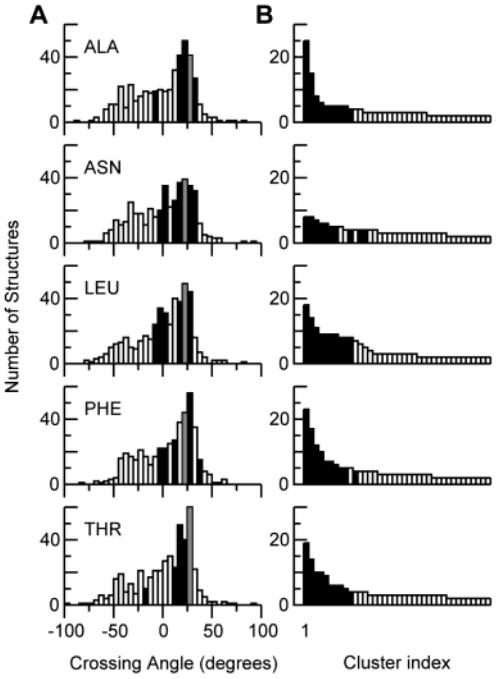

FIGURE 2: Simulated annealing generated 450 dimers of each sequence analyzed, predicting a left-handed coiled coil geometry for all of them. (A) The crossing angles for the ensembles follow bimodal distributions suggestive of ideal packing modes at ~+25 and −35 degrees: left and right-handed coiled coils, respectively. Black bars represent the range in which the top 10 structures fall. Grey bars denote the crossing angles of the top ranked structures. (B) Cluster size distribution. The pure polyleucine sequence exhibits several relatively large clusters, probably due to the surface homogeneity of a pure polyleucine sequence. The *asn* sequence exhibits the widest distribution in structures and the most poorly defined top ranking structures. The incongruity between the top 10 structures and top clusters exhibited by *asn* and *phe* resulted from the symmetry filter during ranking (see Methods).

according to eq 1 as a function of the offset s between the two sets (*71*):

$$cy_1y_2(s) = \frac{\langle (y1_{i+s} - \langle y1\rangle)(y2_i - \langle y2\rangle)\rangle}{\sqrt{\langle (y1_{i+s} - \langle y1\rangle)^2 \langle (y2_i - \langle y2\rangle)^2\rangle}} \quad (1)$$

Gaussian distributed noise was generated with a mean and standard deviation similar to those of the helix rotation data using a modified version of the "Mersenne Twister" random number generator (*72*).

RESULTS

Simulated Annealing. Simulated annealing generated ensembles of 450 structures. Helix−helix crossing angles of dimers in these ensembles followed bimodal distributions with modes at approximately +25° and −35°, corresponding to left- and right-handed structures, respectively (Figure 2A). These structures were clustered, half of the ensemble with the lowest symmetry scores was discarded, and finally members from the top remaining clusters with the lowest potential energies were selected. This resulted in a ranked list of 10 structures that were predominantly left-handed for all the sequences investigated (Figure 2, gray and black bars). The largest clusters contained ~20 members, with the exception of asparagine which gave two smaller clusters containing eight-members each (Figure 2B). The top 10

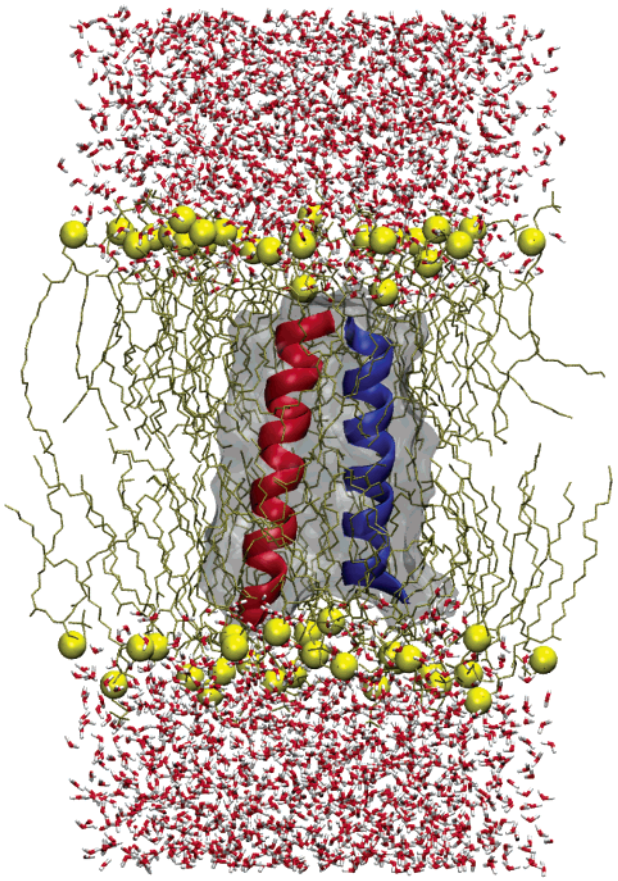

FIGURE 3: Snapshot of the *asn* simulation system after 20 ns of simulation time. This is only one unit cell in an infinite crystal due to the use of periodic boundary conditions to limit edge artifacts. DOPC molecules are shown in stick representation, lipid headgroup phosphorus atoms are yellow spheres, and the peptide surface is shown in gray with ribbon depictions of the monomer backbones superimposed in blue and red. The bilayer is hydrated in water (red and white).

structures had crossing angles close to 20° (Figure 2A, gray bars) and exhibited regular left-handed coiled coil packing as determined by the TWISTER algorithm (*61*). Virtually all of the top clusters were retained after symmetry filtering (Figure 2B, black bars), and the majority of all structures generated (>95% except *ala*, 83%) had the single amino acid substitution within 0.42 nm of at least one atom on the opposite chain, i.e., at least marginally in the interface. This confirms that the model generation procedure, designed to maximize inclusion of mutant residues in the helix−helix interface, was successful.

Simulations in a DOPC Bilayer. Top ranked structures were simulated independently in DOPC bilayers for 20 ns each (Figure 3). The root-mean-squared deviations (RMSD) of peptide backbone atoms from the starting conformations (Figure 4) all reached a maximum of about 0.1 nm within the first nanosecond and remained relatively constant for the remainder of the simulations. The asparagine-containing dimer reached a slightly higher RMSD of about 0.15 nm after ca. 3 ns. All peptides retained their α-helical secondary structure, according to the DSSP algorithm (*69*), with the exception of minor and transient disruptions at the N- and C-termini. Superimposed snapshots of the protein backbone atoms taken every 1 ns over the last 10 ns suggest regions near the helix termini are the most mobile (Figure 5).

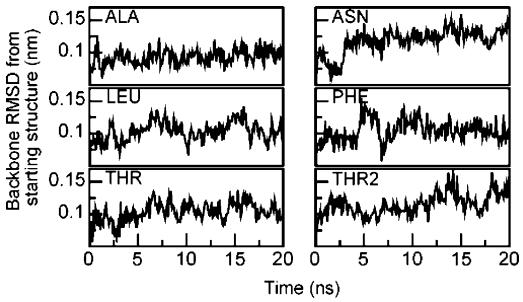

FIGURE 4: The root-mean-squared deviation (RMSD) of the backbone atoms from the starting conformation throughout the simulation. These dimers are all relatively stable, achieving a final RMSD of ∼0.1 nm.

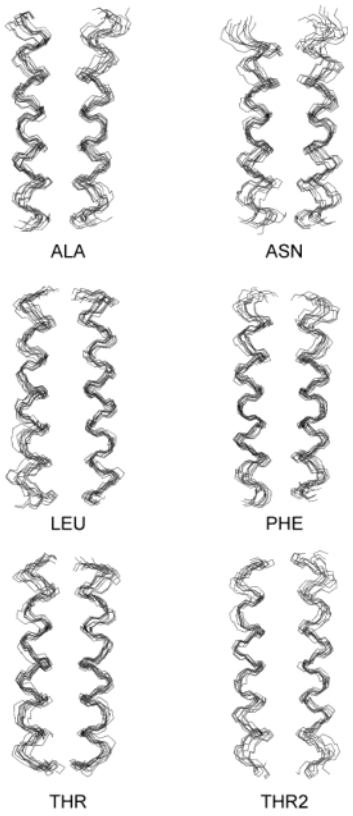

FIGURE 5: Backbone atom snapshots taken every nanosecond for the last 10 ns of the simulations. Structures were aligned by minimizing the RMSD between backbone atoms. The core structures are stable, with *asn* showing the greatest movement of the helices.

Trajectory average radii and crossing angles for all dimers were around 0.5 nm and 20°, respectively, and the packing positions of the mutant residues, denoted by the heptad notation (Figure 1), were invariant throughout all simulations (Table 1). Helix−helix crossing angles typically ranged 10−15° around an average value close to that predicted by simulated annealing (Figure 6), with a standard deviation of ∼3° or ∼15% (Table 1). The *ala* simulation showed a possible slight systematic decrease in the crossing angle, stabilizing over the last 5 ns at around 20°.

The coiled coil radii likewise fluctuated, averaging near 0.5 nm (Figure 7). In all cases except *ala*, the average radius was slightly larger than that predicted by in vacuo simulated annealing. The *thr* simulation, with threonine positioned in the dimer interface, maintained a smaller radius than the other simulations; *thr2* had a polyleucine dimer interface with

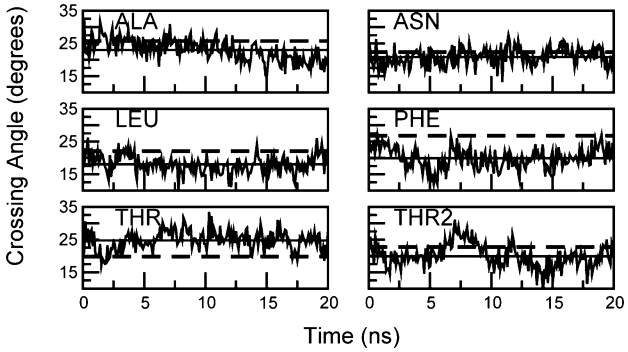

FIGURE 6: Helix−helix crossing angles assigned by the TWISTER algorithm. Straight solid line: Simulation average. Dotted line: Starting structure. Short and longer term fluctuations on the order of 10 to 15 degrees are apparent, but overall they remain close to the average values.

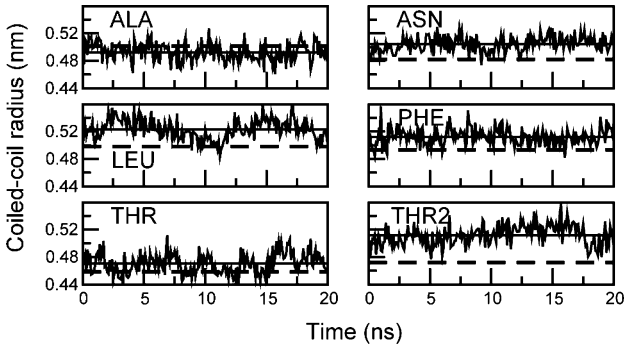

FIGURE 7: Coiled coil radii assigned with the TWISTER algorithm. Straight solid line: Simulation average. Dotted line: Starting structure. These are suggestive of reasonable stability. The *thr* simulation exhibits a notably smaller radius than the other dimers.

threonine lipid exposed, and the radius of this dimer was comparable to the others. The relative fluctuations in radii were smaller than those of the crossing angles, with standard deviations of ∼0.013 nm, or ∼2% (Table 1).

Sequences containing threonine and asparagine in the variable position exhibited both intermolecular and intramolecular hydrogen bonds (Table 2). Threonine was found to predominantly form intramolecular (*i* to *i-4*) hydrogen bonds to the peptide backbone of the helix on which it resided; these persisted ∼85−90% of the time in the *thr* simulation with the threonines situated in the dimer interface and >99% in the *thr2* simulation where threonines were lipid exposed. Intermolecular hydrogen bonds involving threonine side-chains occurred ∼23% of the time in the *thr* simulation; the hydrogen bond acceptor threonine was usually simultaneously involved in an intramolecular hydrogen bond to its own helix backbone. Asparagine partitioned its hydrogen bonds between a variety of inter and intramolecular hydrogen bonds involving both backbone and side-chain atoms, with at least one intermolecular hydrogen bond in existence throughout 99% of the simulation (Table 2). Side-chain to side-chain hydrogen bonds were found throughout 45% of the simulation, and side-chain to backbone intermolecular hydrogen bonds occurred 22 and 30% of the time for each monomer, respectively. Hydrogen bonds between an asparagine side-chain and its own helix backbone were found around 50% of the time.

Hydrogen bond patterns between asparagine-containing helices were typically asymmetric (Figure 8A). Each asymmetric arrangement appeared to persist for a period of approximately 5−7 ns, after which an alternative arrangement would become dominant (Figure 8B). A period between ca. 11.7 and 12.3 ns was devoid of intermolecular side-chain to side-chain or backbone hydrogen bonds, with both asparagine side-chains hydrogen bonding to backbone carbonyl oxygens on their respective helices (Figure 8, region 3). Other regions were typified by various asymmetric arrangements of hydrogen bonds involving side-chain and backbone atoms (Figure 8, regions 1, 2, and 4). Despite the obvious existence of periods with preferred hydrogen bond arrangements, these arrangements were very transient with rapid side-chain rotations and fluctuations occurring at all times.

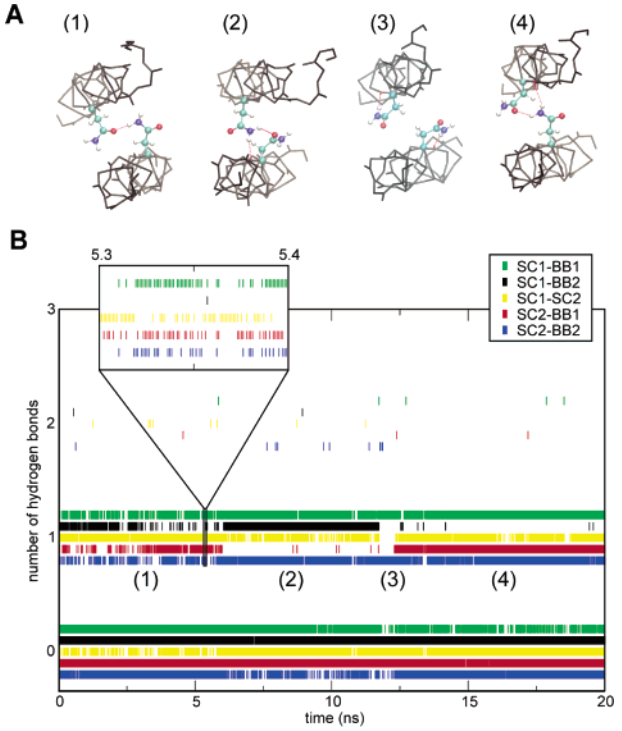

FIGURE 8: Asparagine hydrogen bonds in the *asn* simulation. (A) Snapshots of hydrogen bonding taken at the times indicated in panel B. (1) An asymmetric hydrogen bond between asparagine side-chains. (2) Simultaneous side-chain and backbone hydrogen bonds. (3) A brief period in which no intermolecular hydrogen bonds were present. (4) Similar to (2) but with the role of each monomer reversed. (B) Hydrogen bonds are split into five classes: SC1-BB1, SC1-BB2, SC1-SC2, SC2-BB1, and SC2-BB2. SC: asparagine side-chain atoms. BB: backbone atoms. (1) and (2) denote individual monomers. The number of hydrogen bonds in each class is indicated.

The average crick angle (α, Figure 1), defined in this case over a stretch of seven residues including the variable one, is an unintuitive and unphysical property that allows one to monitor the relative rotational orientation of one helix with respect to the position of the other one. Slight rotations of helices about their axes were identified in all cases (Figure 9A). The magnitude of these rotations depended on the residue type, with the *phe* simulation exhibiting the smallest changes (Figure 9A, standard deviation of this property for *phe*: 1.7°, *ala:* 3.0°, *asn:* 3.2°, *leu:* 3.0°, *thr:* 3.2°, and *thr2:* 4.2°). The cross correlation function (see Methods) allowed the correlation of these rotations to be investigated between the helices in each dimer; a negative correlation coefficient indicated clockwise rotation of one helix is

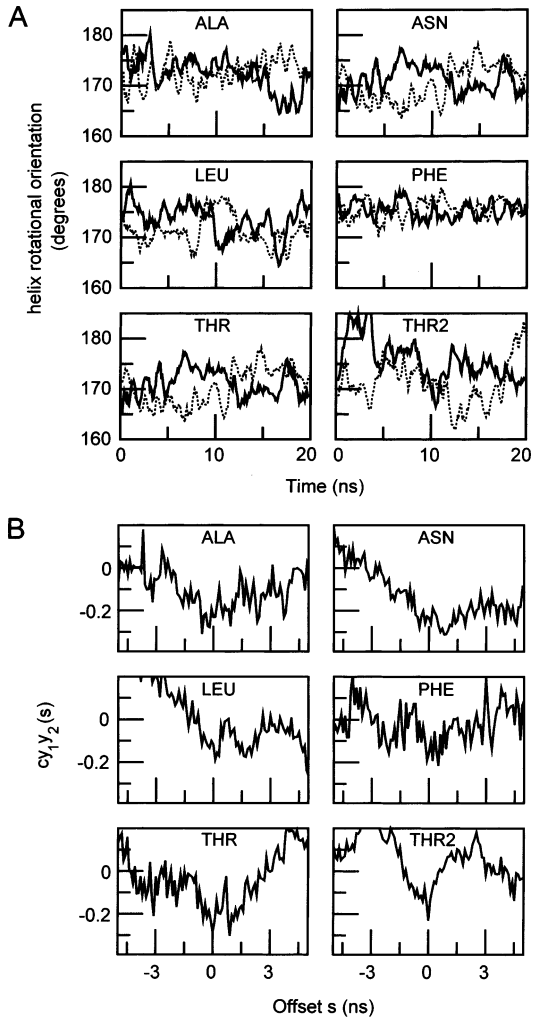

FIGURE 9: (A) Rotation of each helix with time. The average crick angle (α) is an unintuitive property but can indicate relative rotational orientations of the helices. (B) The cross correlation function $cy_1y_2(s)$ indicates motion is most correlated with a time lag s close to 0 ns with a cross correlation coefficient of −0.2 to −0.3, indicating clockwise rotation in one helix is correlated with counterclockwise rotation in the other. For comparison, Gaussian distributed noise with similar statistical properties gives a cross correlation coefficient with a magnitude of about ± 0.07.

Table 3: Cross Correlation Coefficients for the Rotational Motions of Individual Helices in Each Dimer[a]

simulation	$Cy_1y_2(s)$	s (ns)[b]
ala	−0.309	−0.6
asn	−0.311	0.8
leu	−0.189	0.1
phe	−0.215	0.5
thr	−0.303	0.9
thr2	−0.230	0

[a] See eq 1 in main text. [b] This is the offset s corresponding to the minimum in the cross correlation function.

correlated with counterclockwise rotation of the other. All of the simulations exhibited slightly correlated rotations with correlation coefficients between −0.2 and −0.3 (Table 3). Helix rotations were most correlated for *ala* (−0.309), *asn* (−0.311), and *thr* (−0.303). Less correlation was seen for *leu* (−0.189), *phe* (−0.215), and *thr2* (−0.230). A short time lag in the response of one monomer's rotational orientation to the other's, on the order of a few hundred picoseconds, was seen (Table 3). Similar analysis of a computer generated pseudo-random set following a Gaussian distribution with similar statistical properties to the simulation data gave a much lower cross correlation coefficient (∼-0.07) and a much noisier cross correlation function, without the distinct negative peak near the zero offset (Figure 9B).

DISCUSSION

Preferred Geometry of Polyleucine Dimers. A left-handed coiled coil is the predicted arrangement of two 24-residue-long monosubstituted polyleucine transmembrane helices in a DOPC bilayer. The ensemble generated by simulated annealing showed a clear preference for left-handed crossing angles, and the top ranked structure for each sequence was a left-handed coiled coil (Figure 2A). The larger spread of relatively populated clusters exhibited by the pure polyleucine sequence is a result of the homogeneity of a pure polyleucine helix surface (Figure 2B); clustering analysis was based on backbone atom coordinates, not interfacial packing motifs, and thus would differentiate rotationally related structures with otherwise similar coiled coil packing of side-chains.

A number of transmembrane α-helices contains heptad repeats of leucine and other hydrophobic residues (*48*), and this heptad motif is typical of left-handed coiled coils in water-soluble proteins. The bimodal distribution of crossing angles seen in the simulated annealing results (Figure 2A) is consistent with the c_m and a_m classes of helix−helix packing predicted by the helical lattice superposition model of Walther et al. (*73*). This is also supported by an analysis of known membrane protein structures (*50*) with the caveat that the preference for right-handed crossing angles shown by that analysis may be explained by the inclusion of specific dimerization motifs (the right-handed GXXXG motif, for example) that are not represented by pure polyleucine.

It is worth mentioning that a certain amount of bias is introduced by running simulated annealing with an initially parallel orientation, making well-packed structures with smaller absolute crossing angles more accessible. This bias is justified by assuming that hydrophobic α-helices naturally adopt a bilayer-spanning orientation (*12*), and considering the counteracting intrinsic statistical bias toward larger crossing angles between unconstrained helices (*74*, *75*).

These left-handed dimers were stable when simulated in DOPC membranes for 20 ns. The backbone RMSD from the starting structure remained at around 0.1 nm in all cases (Figure 4); small changes arose from minor fluctuations around average structures. The α-helical secondary structure of the peptides did not change (Figure 5). All minor distortions of α-helical structure are near the helix termini at the bilayer/water interface, where competing hydrogen bonds with headgroup atoms and water molecules can disrupt α-helical hydrogen bonds. This is in agreement with circular dichroism measurements that show these peptides form α-helices in SDS micelles (*41*), and the observation that they form stable transmembrane segments in ToxR/polyleucine/MalE chimeras (*42*). The hydrophobic thickness of DOPC is approximately 3.4 nm and a 24-residue α-helix is approximately 3.6 nm long, suggesting an α-helical conformation provides the best hydrophobic match with the bilayer (*40*).

The packing positions of the mutant residues, defined in terms of their crick angles (Figure 1), were invariant during

the simulations (Table 1). Helix−helix crossing angles and radii were likewise stable, showing random fluctuations around well-defined average structures (Table 1, Figures 6 and 7). The average values in all cases are close to those predicted for an ideal coiled coil (*45*). The relative fluctuations in crossing angles were larger than those of the radii, indicating that structural fluctuations are possible without affecting the tight association of helices. In most cases, the average crossing angles were lower than those generated by in vacuo simulated annealing; it has been shown that helix−helix crossing angles can be dependent on the environment (*52*), so this is not unexpected.

Similar simulations on an antiparallel polyleucine dimer (Ash et al., unpublished results) exhibited side-chain packing rearrangements and the formation of a more coiled coil structure from an initially irregular structure with a crossing angle near 0°, suggesting 20 ns is adequate to assess the conformational stability of such dimers.

Dynamic Properties and Structural Flexibility. Helix−helix crossing angles varied throughout the simulation (Figure 6); that of pure polyleucine ranged between ca. 10° and 25°. The relative fluctuations in crossing angles were much larger than those of the radii (as indicated by the standard deviations of these properties, Table 1), demonstrating that conformational flexibility is possible without compromising close association of helices. Some of the simulations show gradual undulations in crossing angle (e.g., *thr2*), whereas others (e.g. *leu*) seem to fluctuate more rapidly around their average value (Figure 6). Longer simulations would be required to assess the significance, if any, of these minor differences.

The systematic decrease in crossing angle observed for *ala* (Figure 6) suggested some packing optimization took place; the radius of this dimer was essentially invariant (Figure 7) so this adaptation did not involve any significant dissociation of the helices. It is known that one or two alanine residues can be incorporated into a polyleucine interface without significantly affecting dimerization (*42*), but the inclusion of four or more alanines dramatically reduces association. It is worth noting that those experiments did not permit the antiparallel orientation of α-helices; other work suggests helices with multiple alanines may preferentially associate in an antiparallel manner consistent with a helix dipole effect (*54*, *55*).

Asparagine appears to destabilize ideal coiled coil packing, possibly to maintain optimum hydrogen bonding geometry. Clustering of the simulated annealing results showed two equally populated top clusters with only eight members each (Figure 2B). A larger distribution of left-handed crossing angles is apparent (Figure 2A). The energetic importance of satisfying hydrogen bonds in a low dielectric environment may result in a larger variety of satisfactory structures, dictated by the balance between van der Waals and hydrogen bonding energies. A comparison of the backbone RMSD during simulation in DOPC to that of the other simulations (Figure 4) and a series of superimposed backbone snapshots (Figure 5) suggests asparagine allows structures that are more loosely packed and more flexible. The ability of asparagine to strongly promote interactions between sterically compatible helices is known (*22*, *23*), but a more recent study in which asparagine was "walked" along the M13 major coat protein (MCP) transmembrane helix demonstrated that helix association driven by asparagine is nevertheless significantly affected by steric compatibility (*76*). It is interesting that the MCP helix contains a glycine motif on one side of the helix. This may provide a stronger force for association than a single asparagine could, suggested by the fact that asparagine only increases association when on the same face of the helix as the glycine residues. The relevance of this observation to hydrophobic helices of more uniform composition, such as those studied by Gurezka and Langosch (*42*), is not clear and is worth further study.

The results of simulated annealing may also simply indicate that asparagine alters the kinetics of structural rearrangement such that convergence to optimal structures requires a longer period of time; it might take a long time to break a hydrogen bond in a vacuum to allow for a thermodynamically favorable structural rearrangement. This dramatic increase in the number of unique structures generated, despite the simplicity of the primary sequence, may underscore a limitation of simulated annealing. Although this method has been used to predict (with good accuracy) the structures of the soluble GCN4 leucine zipper (*51*) and the dimeric transmembrane protein glycophorin A (*59*), there still remains ambiguity in the selection of a single optimum structure. As a test of our simulated annealing procedure, we modeled glycophorin A and identified the NMR structure within the top three ranking structures (depending on the search parameters), but the distribution of structures was much wider than that of the polyleucine sequences studied here (data not shown). It may be more useful to use simulated annealing to generate an ensemble of structures for statistical analysis than to simply develop a single static structural model.

Hydrogen Bonding Involving Asparagine and Threonine. Threonine appears to promote the closer association of polyleucine transmembrane helices. In the *thr* simulation, where threonine is located in the dimer interface, the average coiled coil radius was 0.47 nm, significantly lower than those of the other simulations (Table 1). Although threonine is smaller than many of the other residues, a comparison to the radius of the alanine containing dimer (0.49 nm) suggests small size is not sufficient to draw the helices closer together. Threonine does not have multiple hydrogen bond donors and acceptors such as asparagine, but it is still capable of forming interstrand hydrogen bonds a significant fraction of the time (23%, Table 2) with a concomitant reduction in intramolecular hydrogen bonding. For most of the simulation, threonine interacted in an intramolecular *i* to *i-4* pattern typical of hydroxyl-containing amino acids (*50*). Together these observations help explain why a single threonine does not promote aggregation of polyleucine in vivo (*23*), but motifs containing multiple serine or threonine residues can (*39*). It appears possible that a single threonine in the appropriate position can induce tighter association of helices as a result of hydrogen bonding, but this force is not strong enough to significantly increase the propensity of pure polyleucine to dimerize, unless it acts in several positions.

Asparagine was involved in one or more intermolecular hydrogen bonds for 99% of the entire simulation (Table 2). Asparagine also participated in hydrogen bonds with partner backbone atoms ∼25% of the time, unlike threonine, which never hydrogen bonded to the opposite backbone (Table 2). Typical hydrogen bonding patterns involved at least one side-

chain to side-chain contact (Figure 8, region 1) and a contact with the opposite backbone (Figure 8, regions 4 and 2). Intramolecular side-chain−backbone interactions were recurrent but transient (Figure 8B), reforming continuously throughout the simulation for a total of ∼50% of the total simulation time (Table 2). A period between ca. 11.7 and 12.3 ns was devoid of any intermolecular hydrogen bonds (Figure 8B, region 3). This period comprised a symmetric structure with each asparagine hydrogen-bonded to one peptide backbone oxygen; in contrast, intermolecular hydrogen bonding arrangements observed were typically asymmetric (Figure 8A). Rapid hydrogen bond breaking, side-chain reorientation, and reformation were apparent throughout the trajectory, but there appear to be regions in which a particular hydrogen bonding arrangement is favored (Figure 8B). Shifts between favored asymmetric arrangements occurred approximately every 5−7 ns.

Steric and conformational constraints (due to dimer configuration, adjacent side-chains, and the surrounding lipids) may preclude the formation of symmetric hydrogen bonding between side-chains, although it is possible that other structural configurations exist but were not observed in this simulation. A large simulation conducted by us containing 36 MS1 helices in a bilayer-mimetic octane slab shows many instances of both symmetric and asymmetric hydrogen bonding between monomers, with a coiled coil radius between ∼0.45 and ∼0.65 nm (*77*). However, in this system symmetric and asymmetric arrangements of hydrogen bonding do not interconvert in the time scale of the simulation (45 ns).

These observations are in agreement with numerous experiments demonstrating the high propensity for asparagine (as well as glutamine, glutamate, and aspartate), but not threonine, to promote oligomerization of transmembrane helices (*22*, *23*, *39*). Asparagine has the ability to form numerous different hydrogen bonds involving both side-chain and backbone atoms, often simultaneously, which could provide a driving force for helix−helix association.

Coordinated Helix Rotations. In all simulations, minimal changes in the helix-packing interfaces were observed, but small-scale coordinated rotations of helices about their axes were identified (Figure 9). These motions could be described as helices rattling back and forth in a gear-like manner, with counterclockwise rotations in one helix moderately correlated with clockwise rotations in the other. The magnitude of these rotations depended on residue type, with the *phe* simulation exhibiting the smallest changes. This suggests that bulky side-chains can limit rotation by locking the dimer into a more rigid conformation. It may be possible to exploit this effect to therapeutically modulate membrane protein function, for example, by introducing a bulky hydrophobic drug molecule with tight affinity into a position that could restrict rotational motion of an important helix.

The greatest rotational correlation was seen between monomers in the *ala*, *asn*, and *thr* simulations, all of which exhibited a correlation coefficient of around −0.3 (Table 3). The other simulations, *leu*, *phe*, and *thr2* had significantly smaller correlation coefficients of around −0.2. This suggests that intermolecular hydrogen bonding (and perhaps weak backbone interactions in the case of *ala*) increases the orientational correlation of those helices containing residues capable of forming them.

Helix rotations are proposed to be involved in activation of the ErbB2 receptor (*35*) and the recently proposed mechanism for gating of the acetylcholine receptor (*78*), so coordinated rotations such as these may be important for the activity of other membrane proteins. This suggests an interesting way by which conformational changes could be communicated between neighboring transmembrane helices in receptors and other membrane proteins. It also has implications for the folding of membrane proteins via the two-stage model, suggesting one mechanism by which associated helices may adjust themselves to achieve the final folded arrangement. The energetic barriers to this sort of rotation would be worth further theoretical or experimental characterization.

CONCLUSIONS

Coiled coil dimers of polyleucine are stable in DOPC for at least 20 ns, and a certain amount of conformational flexibility is possible without disrupting tight packing. The single substitutions to alanine, phenylalanine, asparagine, and threonine appear compatible with a polyleucine coiled coil helix interaction interface. Asparagine participates in transient but recurrent inter- and intramolecular hydrogen bonds, and appears to slightly destabilize specific packing of apolar residues in favor of maintaining optimum hydrogen bonding. Threonine mainly forms intramolecular hydrogen bonds in a characteristic *i* to *i-4* (side-chain to backbone) pattern, and only one type of intermolecular hydrogen bond is observed. Threonine promoted closer association of the helices than any other residue, probably because it is both relatively small and can form hydrogen bonds. The higher frequency and number of intermolecular hydrogen bonds formed by asparagine relative to threonine explains the experimentally determined dramatic increase in dimer stability afforded by the former over the latter.

Monomers were observed to chaotically rotate about their helical axes in a slightly correlated manner that is inhibited by phenylalanine. These rotations could play a role in the activity of membrane proteins (*35*, *78*), and may also be a mechanism by which membrane proteins search for the best conformation during protein folding. The role of hydrogen bonding residues in coupling helix rotations is worth further examination.

Limitations imposed by the very slow dynamics of lipid bilayers preclude a thermodynamic analysis of the stability of these coiled coils, but the use of free energy perturbation techniques (*79*) may allow more rigorous thermodynamic treatments in future studies, particularly as computer power increases.

REFERENCES

1. Gether, U. (2000) Uncovering molecular mechanisms involved in activation of G protein-coupled receptors, *Endocr. Rev. 21*, 90−113.
2. Bertaccini, E., and Trudell, J. R. (2002) Predicting the transmembrane secondary structure of ligand-gated ion channels, *Protein Eng. 15*, 443−453.
3. Jiang, Y. X., Lee, A., Chen, J. Y., Ruta, V., Cadene, M., Chait, B. T., and MacKinnon, R. (2003) X-ray structure of a voltage-dependent K+ channel, *Nature 423*, 33−41.
4. Tate, C. G., Kunji, E. R. S., Lebendiker, M., and Schuldiner, S. (2001) The projection structure of EmrE, a proton-linked multidrug transporter from *Escherichia coli*, at 7 angstrom resolution, *EMBO J. 20*, 77−81.

5. Arkin, I. T. (2002) Structural aspects of oligomerization taking place between the transmembrane alpha-helices of bitopic membrane proteins, *Biochim. Biophys. Acta-Biomembr. 1565*, 347−363.
6. Chamberlain, A. K., Faham, S., Yohannan, S., and Bowie, J. U. (2003) in *Membrane Proteins* (Rees, D. C., Ed.) pp 19−46, Elsevier Science (USA), San Diego, California.
7. Popot, J. L., and Engelman, D. M. (2000) Helical membrane protein folding, stability, and evolution, *Annu. Rev. Biochem. 69*, 881−922.
8. von Heijne, G. (1992) Membrane protein structure prediction. Hydrophobicity analysis and the positive-inside rule, *J. Mol. Biol. 225*, 487−494.
9. von Heijne, G. (1999) A day in the life of Dr. K. or how I learned to stop worrying and love lysozyme: A tragedy in six acts, *J. Mol. Biol. 293*, 367−379.
10. Edwards, R. A., and Turner, R. J. (1998) Alpha-periodicity analysis of small multidrug resistance (SMR) efflux transporters, *Biochem. Cell. Biol. 76*, 791−797.
11. Stevens, T. J., and Arkin, I. T. (2001) Substitution rates in alpha-helical transmembrane proteins, *Protein Sci. 10*, 2507−2517.
12. Popot, J. L., and Engelman, D. M. (1990) Membrane protein folding and oligomerization: the two-stage model, *Biochemistry 29*, 4031−4037.
13. Engelman, D. M., Chen, Y., Chin, C.-N., Curran, A. R., Dixon, A. M., Dupuy, A. D., Lee, A. S., Lehnert, U., Matthews, E. E., Reshetnyak, Y. K., Senes, A., and Popot, J. L. (2003) Membrane protein folding: beyond the two stage model, *FEBS Lett. 555*, 122−125.
14. Sansom, M. S. P., and Weinstein, H. (2000) Hinges, swivels and switches: the role of prolines in signalling via transmembrane alpha-helices, *Trends Pharmacol. Sci. 21*, 445−451.
15. Sato, H., Takeda, K., Tani, K., Hino, T., Okada, T., Nakasako, M., Kamiya, N., and Kouyama, T. (1999) Specific lipid−protein interactions in a novel honeycomb lattice structure of bacteriorhodopsin, *Acta Crystallogr. D55*, 1251−1256.
16. White, S. H., and Whimley, W. C. (1999) Membrane Protein Folding and Stability: Physical Principles, *Annu. Rev. Biophys. Biomol. Struct. 28*, 319−365.
17. Liang, J. (2002) Experimental and computational studies of determinants of membrane-protein folding, *Curr. Opin. Chem. Biol. 6*, 878−884.
18. Curran, A. R., and Engelman, D. M. (2003) Sequence motifs, polar interactions and conformational changes in helical membrane proteins, *Curr. Opin. Struct. Biol. 13*, 412−417.
19. Lagüe, P., Zuckermann, M. J., and Roux, B. (2000) Lipid-Mediated Interactions between Intrinsic Membrane Proteins: A Theoretical Study Based on Integral Equations, *Biophys. J. 79*, 2867−2879.
20. Liu, W., Crocker, E., Siminovitch, D. J., and Smith, S. O. (2003) Role of side-chain conformational entropy in transmembrane helix dimerization of glycophorin A, *Biophys. J. 84*, 1263−1271.
21. Kralchevsky, P. A., and Nagayama, K. (2000) Capillary interactions between particles bound to interfaces, liquid films and biomembranes, *Adv. Colloid Interface Sci. 85*, 145−192.
22. Gratkowski, H., Lear, J. D., and DeGrado, W. F. (2001) Polar side chains drive the association of model transmembrane peptides, *Proc. Natl. Acad. Sci. U.S.A. 98*, 880−885.
23. Zhou, F. X., Merianos, H. J., Brunger, A. T., and Engelman, D. M. (2001) Polar residues drive association of polyleucine transmembrane helices, *Proc. Natl. Acad. Sci. U.S.A. 98*, 2250−2255.
24. Smith, S. O., Smith, C. S., and Bormann, B. J. (1996) Strong hydrogen bonding interactions involving a buried glutamic acid in the transmembrane sequence of the neu/erbB-2 receptor, *Nat. Struct. Biol. 3*, 252−258.
25. Bargmann, C. I., Hung, M. C., and Weinberg, R. A. (1986) Multiple independent activations of the neu oncogene by a point mutation altering the transmembrane domain of p 185, *Cell 45*, 649−657.
26. Partridge, A. W., Melnyk, R. A., and Deber, C. M. (2002) Polar residues in membrane domains of proteins: Molecular basis for helix-helix association in a mutant CFTR transmembrane segment, *Biochemistry 41*, 3647−3653.
27. Adams, P. D., Engelman, D. M., and Brunger, A. T. (1996) Improved prediction for the structure of the dimeric transmembrane domain of glycophorin A obtained through global searching, *Proteins 26*, 257−261.
28. Torres, J., Briggs, J. A. G., and Arkin, I. T. (2002) Contribution of energy values to the analysis of global searching molecular dynamics simulations of transmembrane helix bundles, *Biophys. J. 2002*, 6.
29. Sansom, M. S. P., Sankararamakrishnan, R., and Kerr, I. D. (1995) Modeling membrane proteins using structural restraints, *Nat. Struct. Biol. 2*, 624−631.
30. Capener, C. E., Proks, P., Ashcroft, F. M., and Sansom, M. S. P. (2003) Filter flexibility in a mammalian K channel: Models and simulations of Kir6.2 mutants, *Biophys. J. 84*, 2345−2356.
31. Law, R. J., Tieleman, D. P., and Sansom, M. S. P. (2003) Pores formed by the nicotinic receptor M2 delta peptide: A molecular dynamics simulation study, *Biophys. J. 84*, 14−27.
32. Campbell, J. D., Biggin, P. C., Baaden, M., and Sansom, M. S. P. (2003) Extending the structure of an ABC transporter to atomic resolution: Modeling and simulation studies of MsbA, *Biochemistry 42*, 3666−3673.
33. Tieleman, D. P., Hess, B., and Sansom, M. S. P. (2002) Analysis and evaluation of channel models: Simulations of alamethicin, *Biophys. J. 83*, 2393−2407.
34. Fleishman, S. J., and Ben-Tal, N. (2002) A novel scoring function for predicting the conformations of tightly packed pairs of transmembrane alpha-helices, *J. Mol. Biol. 321*, 363−378.
35. Fleishman, S. J., Schlessinger, J., and Ben-Tal, N. (2002) A putative molecular-activation switch in the transmembrane domain of erbB2, *Proc. Natl. Acad. Sci. U.S.A. 99*, 15937−15940.
36. Choma, C. T., Tieleman, D. P., Cregut, D., Serrano, L., and Berendsen, H. J. C. (2001) Towards the design and computational characterization of a membrane protein, *J. Mol. Graphics Modell. 20*, 219−234.
37. DeGrado, W. F., Gratkowski, H., and Lear, J. D. (2003) How do helix-helix interactions help determine the folds of membrane proteins? Perspectives from the study of homo-oligomeric helical bundles, *Protein Sci. 12*, 647−665.
38. Choma, C., Gratkowski, H., Lear, J. D., and DeGrado, W. F. (2000) Asparagine-mediated self-association of a model transmembrane helix, *Nat. Struct. Biol. 7*, 161−166.
39. Dawson, J. P., Weinger, J. S., and Engelman, D. M. (2002) Motifs of serine and threonine can drive association of transmembrane helices, *J. Mol. Biol. 316*, 799−805.
40. de Planque, M. R. R., and Killian, J. A. (2003) Protein−lipid interactions studied with designed transmembrane peptides: role of hydrophobic matching and interfacial anchoring, *Mol. Membr. Biol. 20*, 271−284.
41. Zhou, F. X., Cocco, M. J., Russ, W. P., Brunger, A. T., and Engelman, D. M. (2000) Interhelical hydrogen bonding drives strong interactions in membrane proteins, *Nat. Struct. Biol. 7*, 154−160.
42. Gurezka, R., and Langosch, D. (2001) In vitro selection of membrane-spanning leucine zipper protein−protein interaction motifs using POSSYCCAT, *J. Biol. Chem. 276*, 45580−45587.
43. Davis, J. H., Donna, M. C., Hodges, R. S., and Bloom, M. (1983) Interaction of a Synthetic Amphiphilic Polypeptide and Lipids in a Bilayer Structure, *Biochemistry 22*, 5298−5305.
44. O'Shea, E. K., Klemm, J. D., Kim, P. S., and Alber, T. (1991) X-ray structure of the GCN4 leucine zipper, a two-stranded, parallel coiled coil, *Science 254*, 539−544.
45. Crick, F. H. C. (1953) The packing of alpha-helices: simple coiled-coils, *Acta Crystallogr. 6*, 689−697.
46. Newman, J. R. S., and Keating, A. E. (2003) Comprehensive identification of human bZIP interactions with coiled-coil arrays, *Science 300*, 2097−2101.
47. Lear, J. D., Gratkowski, H., Adamian, L., Liang, J., and DeGrado, W. F. (2003) Position-dependence of stabilizing polar interactions of asparagine in transmembrane helical bundles, *Biochemistry 42*, 6400−6407.
48. Gurezka, R., Laage, R., Brosig, B., and Langosch, D. (1999) A heptad motif of leucine residues found in membrane proteins can drive self-assembly of artificial transmembrane segments, *J. Biol. Chem. 274*, 9265−9270.
49. Walshaw, J., and Woolfson, D. N. (2001) SOCKET: A program for identifying and analysing coiled-coil motifs within protein structures, *J. Mol. Biol. 307*, 1427−1450.
50. Bywater, R. P., Thomas, D., and Vriend, G. (2001) A sequence and structural study of transmembrane helices, *J. Comput.-Aided Mol. Des. 15*, 533−552.
51. Nilges, M., and Brunger, A. T. (1993) Successful prediction of the coiled coil geometry of the GCN4 leucine zipper domain by

simulated annealing: comparison to the X-ray structure, *Proteins 15*, 133−146.
52. Petrache, H. I., Grossfield, A., MacKenzie, K. R., Engelman, D. M., and Woolf, T. B. (2000) Modulation of glycophorin A transmembrane helix interactions by lipid bilayers: Molecular dynamics calculations, *J. Mol. Biol. 302*, 727−746.
53. Smith, S. O., Eilers, M., Song, D., Crocker, E., Ying, W. W., Groesbeek, M., Metz, G., Ziliox, M., and Aimoto, S. (2002) Implications of threonine hydrogen bonding in the glycophorin A transmembrane helix dimer, *Biophys. J. 82*, 2476−2486.
54. Gernert, K. M., Surles, M. C., Labean, T. H., Richardson, J. S., and Richardson, D. C. (1995) The Alacoil: a very tight, antiparallel coiled-coil of helices, *Protein Sci. 4*, 2252−2260.
55. Fujita, K., Bunjes, N., Nakajima, K., Hara, M., Sasabe, H., and Knoll, W. (1998) Macrodipole interaction of helical-peptides in a self-assembled monolayer on gold substrate, *Langmuir 14*, 6167−6172.
56. Smith, S. O., Smith, C., Shekar, S., Peersen, O., Ziliox, M., and Aimoto, S. (2002) Transmembrane interactions in the activation of the Neu receptor tyrosine kinase, *Biochemistry 41*, 9321−9332.
57. Brunger, A. T., Adams, P. D., Clore, G. M., DeLano, W. L., Gros, P., Grosse-Kunstleve, R. W., Jiang, J. S., Kuszewski, J., Nilges, M., Pannu, N. S., Read, R. J., Rice, L. M., Simonson, T., and Warren, G. L. (1998) Crystallography & NMR system: A new software suite for macromolecular structure determination, *Acta Crystallogr. D54*, 905−921.
58. Kaminski, G. A., Friesner, R. A., Tirado-Rives, J., and Jorgensen, W. L. (2001) Evaluation and reparametrization of the OPLS-AA force field for proteins via comparison with accurate quantum chemical calculations on peptides, *J. Phys. Chem. B 105*, 6474−6487.
59. Treutlein, H. R., Lemmon, M. A., Engelman, D. M., and Brunger, A. T. (1992) The glycophorin-A transmembrane domain dimer − sequence-specific propensity for a right-handed supercoil of helices, *Biochemistry 31*, 12726−12733.
60. Kelly, L. A., Gardner, S. P., and Sutcliffe, M. J. (1996) An automated approach for clustering an ensemble of NMR-derived protein structures into conformationally related subfamilies, *Protein Eng. 9*, 1063−1065.
61. Strelkov, S. V., and Burkhard, P. (2002) Analysis of alpha-Helical Coiled Coils with the Program TWISTER Reveals a Structural Mechanism for Stutter Compensation, *J. Struct. Biol. 137*, 54−64.
62. Lindahl, E., Hess, B., and van der Spoel, D. (2001) GROMACS 3.0: a package for molecular simulation and trajectory analysis, *J. Mol. Model 7*, 306−317.
63. Berger, O., Edholm, O., and Jahnig, F. (1997) Molecular dynamics simulations of a fluid bilayer of dipalmitoylphosphatidylcholine at full hydration, constant pressure, and constant temperature, *Biophys. J. 72*, 2002−2013.
64. van der Spoel, D., van Buuren, A. R., Apol, E., Muelenhoff, P. J., Tieleman, D. P., Sijbers, A. L. T. M., Hess, B., Feenstra, K. A., Lindahl, E., van Drunen, R., and Berendsen, H. J. C. (2002) Gromacs User Manual Version 3.1.1, University of Groningen, Groningen, NL.
65. Essmann, U., Perera, L., Berkowitz, M. L., Darden, T., Lee, H., and Pedersen, L. G. (1995) A smooth particle mesh ewald method, *J. Chem. Phys. 103*, 8577−8593.
66. Berendsen, H. J. C., Postma, J. P. M., van Gunsteren, W. F., DiNola, A., and Haak, J. R. (1984) Molecular Dynamics with coupling to an external bath, *J. Chem. Phys. 81*, 3684−3690.
67. Faraldo-Gomez, J. D., Smith, G. R., and Sansom, M. S. P. (2002) Setting up and optimization of membrane protein simulations, *Eur. Biophys. J. Biophy. 31*, 217−227.
68. Sanner, M. F., Olson, A. J., and Spehner, J. C. (1996) Reduced surface: An efficient way to compute molecular surfaces, *Biopolymers 38*, 305−320.
69. Kabsch, W., and Sander, C. (1983) Dictionary of protein secondary structure: pattern recognition of hydrogen-bonded and geometrical features, *Biopolymers 22*, 2577−2637.
70. Humphrey, W., Dalke, A., and Schulten, K. (1996) VMD − Visual Molecular Dynamics, *J. Mol. Graphics 14*, 33−38.
71. Leach, A. R. (2001) *Molecular Modelling: Principles and Applications*, 2 ed., Pearson Education Limited, Essex, England.
72. Matsumoto, M., and Nishimura, T. (1998) Mersenne Twister: A 623-dimensionally equidistributed uniform psuedorandom number generator, *ACM Trans. Modell. Comp. Simul. 8*, 3−30.
73. Walther, D., Eisenhaber, F., and Argos, P. (1996) Principles of helix-helix packing in proteins: The helical lattice superposition model, *J. Mol. Biol. 255*, 536−553.
74. Walther, D., Springer, C., and Cohen, F. E. (1998) Helix-helix packing angle preferences for finite helix axes, *Proteins 33*, 457−459.
75. Bowie, J. U. (1997) Helix packing angle preferences, *Nat. Struct. Biol. 4*, 915−917.
76. Dawson, J. P., Melnyk, R. A., Deber, C. M., and Engelman, D. M. (2003) Sequence Context Strongly Modulates Association of Polar Residues in Transmembrane Helices, *J. Mol. Biol. 331*, 255−262.
77. Stockner, T., Ash, W. L., MacCallum, J. L., and Tieleman, D. P. (2004) Direct simulation of transmembrane helix association: role of asparagines. *Biophys. J.*, in press.
78. Miyazawa, A., Fujiyoshi, Y., and Unwin, M. (2003) Structure and gating mechanism of the acetylcholine receptor pore, *Nature 423*, 949−955.
79. Kollman, P. (1993) Free-energy calculations − applications to chemical and biochemical phenomena, *Chem. Rev. 93*, 2395−2417.

BI0494572